Research Article Vol. 14, No. 11 / 1 Nov 2024 / Optical Materials Express 2542
Optical Materials EXPRESS

Fluorine fluid experimental determination of the refractive index, spectral and thermal variation, and transparency quantification of the MezzoCielo telescope

Silvio Di Rosa,[1,*] Roberto Ragazzoni,[1,2] Maria G. Pelizzo,[3,4] Alain J. Corso,[4] Giovanni Santi,[4] Carmelo Arcidiacono,[2] Demetrio Magrin,[2] Marco Dima,[2] Jacopo Farinato,[2] and Simone Zaggia[2]

[1]University of Padua, Department of Physics and Astronomy, Via 8 Febbraio, Padua 35122, Italy
[2]Italian Institute for Astrophysics (INAF), Vicolo dell'Osservatorio 5, Padua 35122, Italy
[3]University of Padua, Department of Information Engineering, Via Gradenigo 6B, Padua 35131, Italy
[4]Consiglio Nazionale delle Ricerche (CNR), Via Trasea 7, Padua 35131, Italy
[*]silvio.dirosa@inaf.it

Abstract: The MezzoCielo (or "half of the sky") is a telescope that aims to revolutionize the way astronomical observations are carried out: once operational, it will be able to continuously patrol the whole sky due to its extremely large field of view estimated to be around 10^4 square degrees, showing, at the same time, the spatial resolution required for scientific purposes. It is a monocentric optical device designed on the concept of an optical sphere; the latter requires the filling of its inner volume with special fluid in order to be actually convergent with a reasonable focal ratio (for spherical aberration reduction). This fluid must exhibit two main properties, namely, a low refractive index and an extremely high transparency in the visible range. In addition, many other characteristics are also required: thermal and chemical stability over time, no toxicity or flammability, and compatibility with glass and metals are some examples. On the basis of these considerations, two fluorine liquids have been selected: the fluids commercially known as FC-72, perfluorohexane with $n_d = 1.251$ at $T = 25°C$, and Novec7200, ethoxy-nonafluorobutane with $n_d = 1.282$ at $T = 25°C$. In this work, the experimental evaluation of their optical properties (refractive index and transparency) in the visible range and in the thermal interval [-10,+25]°C has been carried out in order to verify the data supplied by the manufacturer and to fully characterize their optical behaviour both spectrally and thermally. All the employed techniques have been firstly applied to commercial pure water, for which extensive literature could be used as reference for the procedures validation.

1. Introduction

A revolution in the way of doing astronomy is based primarily upon the invention of innovative types of optical systems. Their advanced optical performance is due to the adoption of new configurations and/or the implementation of novel components. In this work, the use of commercial liquids allows the realization of liquid monocentric lens of low refracting index, namely it allows to realize the MezzoCielo telescope, which is characterized by an unprecedented value of the Field of View, around ten thousand square degrees [1].

The primary lens of MezzoCielo telescope is supposed to be a 2-meter diameter sphere constituted by a 12-centimeter thickness outer shell made of a common glass, likely BK7, which encloses an inner cavity, as shown in Fig. 1[1,2].

#531842 https://doi.org/10.1364/OME.531842
Journal © 2024 Received 3 Jun 2024; revised 23 Jul 2024; accepted 23 Jul 2024; published 7 Oct 2024

Optical Materials EXPRESS

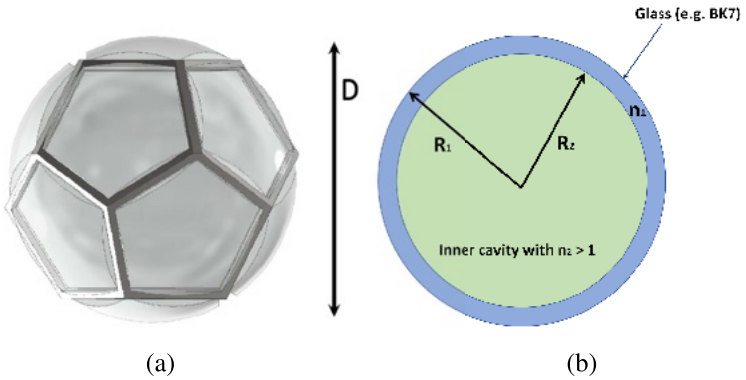

(a) (b)

Fig. 1. Schematic representation of the MezzoCielo assembly: (a) rendering of the actual telescope structure, resembling that of a Platonic solid, such as a dodecahedral one; (b) bidimensional sketch of the monocentric lens cross-section, in which the geometrical and optical main properties, namely its spherical optical nature, the outer and inner radius R_1 and R_2, the glass shell and the fluid volume with refractive indices of n_1 and n_2 respectively, are highlighted.

Optical calculations have clearly demonstrated that the refractive index of the inner material has to be greater than one in order to make the optical power of the lens positive, but, at the same time, it should be relatively low to maintain an adequate focal length for this application [1]. The focal length f of a monocentric lens composed by a shell of refractive index n_1 and an inner sphere of refractive index n_2 is:

$$f = \frac{R_1 R_2 n_1 n_2}{2(n_1 - 1)R_2 n_2 + 2(n_2 - n_1)R_1}, \tag{1}$$

with R_1 radius of the whole lens and R_2 radius of the inner sphere. Since, for reasons of mechanical stability, the shell must be divided into identical sectors supported by a mechanical structure (Fig. 1(a)) [3], the telescope focal ratio is given by

$$\text{F} - \text{number} = \frac{f}{\eta D} = \frac{f}{\eta 2R_1}, \tag{2}$$

where the filling factor η takes into account the effects of the mechanical supporting structure on the telescope aperture. While the reduction of the spherical aberration requires a relatively high focal length, the achievement of the target Field of View is possible only with low F-number; once the lens diameter is set, its focal length depends upon the liquid refractive index, increasing as the index decreases. It has been found that an F-number value of around 2.5 provides a good balance between the desired Field of View and the spherical aberration reduction. Supposing a filling factor equal to 0.5, a focal ratio of 2.5 requires, for a 2-meter sphere with shell thickness of 12-centimeter, a value of around $n_2 = 1.28$ for the material refractive index inside the inner cavity. Consequently, indexes between 1.2 and 1.3 are considered for the MezzoCielo optical bulk.

Such values of refractive index, together with other requirements (high transmissibility in the visible spectrum, low density, possibility of handling without hazards, mass production at low cost) have led to take into account liquid materials and, among them, two fluorine fluids have been found to be the most promising: perfluorohexane C_6F_{14} and ethoxy-nonafluorobutane $C_6H_5F_9O$. These fluids, commercially available and known as FC-72 and Novec7200 respectively, are currently used in the electronics field as heat transfer liquids, but there is no evidence of a their utilization for astronomical purposes. As a consequence, in their datasheets (retrievable in

Optical Materials EXPRESS

Refs. [4] and [5]), while the main thermo-mechanical properties are listed (for example, density, which is around 1670 kg/m^3 for the FC-72 and 1420 kg/m^3 for Novec7200 at room temperature), the only optical information regards the refractive index, reported as a single value, 1.251 and 1.282 respectively for FC and Novec. The fact that the liquids are transparent is stated as well, but without any quantification. In order to finalize the telescope optical design and detailing its overall efficiency, it's mandatory to know both the refractive index spectral and thermal variation, along with the quantification of transparency in the visible range.

Therefore, this work explores the novel possible use of fluorine fluids for optical and astronomical purposes by providing for the first time the refractive index values and their dependency on temperature. Such data will be fundamental in sizing the telescope itself. In addition, they could be useful also to many other applications requiring thermally stable, low refractive index, extremely high transparency materials for advance optical components.

2. Materials and methods

Refractive index and transparency calculations for the two liquids, FC-72 and Novec7200, are described in this section. These techniques have also been applied to the estimation of the optical properties of pure water, employed as reference material.

2.1. Refractive index evaluation

The experimental determination of the liquids refractive index is based upon the procedure illustrated in Ref. [6]. The idea is to measure the size of the image of a known object formed by liquid refraction and compare it to the actual object size: the amount of magnification is proportional to the refractive index itself. In addition, we managed to modify the refractive index measurement technique by introducing, in the experimental set-up, several Wratten filters in order to characterize the refractive index in the visible range, as it will be discussed in Sec. 2.2. According to Ref. [6], a beaker (B) and a graduated cylinder (C) are employed to perform the evaluation. The first one is used as a vessel for the liquid, the second one as the object whose image size has to be measured. Their diameters are chosen in order to fulfill the following condition:

$$d_B > \frac{n}{n_0} d_C, \tag{3}$$

with n liquid refractive index, n_0 air refractive index (supposed equal to 1), d_B and d_C beaker and cylinder outer diameter respectively. Since in our set-up $d_B \approx 2.1 d_C$, with liquid refractive index supposedly not greater than 1.3, the condition expressed by Eq. (3) is always satisfied. The graduated cylinder was inserted inside the beaker and made concentric with the latter using a 3D printed stabilizer element. The liquids (one at time) have been then poured into the annular cavity between C and B. A sketch of the assembly is depicted in Fig. 2.

In Fig. 2, the image of the cylinder produced by fluid refraction is denoted with C'. At this point, the liquid refractive index can be approximated using the following relation:

$$n = \frac{d_{C'}}{d_C} n_0 \approx \frac{d_{C'}}{d_C}, \tag{4}$$

where $d_{C'}$ represents the diameter of the cylinder image. In other words, the calculation of n is led back, using Eq. (4), to the obtainment of $d_{C'}$. The latter, in turn, can be measured upon photos of the experimental assembly. For this purpose, the CANON 5d EOS camera has been employed and set in front of the beaker-liquid-cylinder assembly in such a way that liquid is at the center of the camera Field of View. Moreover, a lamp has been located in the proximity of the arrangement in order to increase the illumination conditions and the definition of the photos. The experimental set-up appears as reported in Fig. 3.

After taking the photos, they have been transferred on a personal computer using a storage unit. With the aid of the *Inkscape* software, it was then possible to measure the required length.

Optical Materials EXPRESS

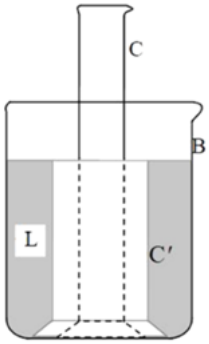

Fig. 2. Sketch of the experimental device [6].

Fig. 3. Experimental set-up employed for the refractive index calculation.

2.2. Refractive index spectral variation

In order to obtain the complete evolution of n within the spectrum of wavelengths from 400 to 700 nm, the following *Wratten* filters have been used:

1. Filter N. 35;
2. Filter N. 47;
3. Filter N. 11;
4. Filter N. 12;
5. Filter N. 21;
6. Filter N. 33.

Optical Materials EXPRESS

Located in front of the camera, they allow associating the refractive index, calculated from the photos, to a specific wavelength, that is the barycentric wavelength resulting from the combined transmission curve of the arrangement camera detector + filter. The transmission curve of the CANON 5d EOS can be easily retrieved from several websites, like Ref. [7], as well as the filters one [8]. Knowing the transmissibility of each device, it's then possible to calculate the barycentric wavelength λ_{bar} of the combination camera + filter. Indicating with $T_{canon}(\lambda)$ and with $T_{filter}(\lambda)$ respectively the transmittances of the camera and the single filter, λ_{bar} can be determined as follows:

$$T_{total} = \sum_{i=400}^{700} T_{canon}(\lambda_i) T_{filter}(\lambda_i), \tag{5}$$

$$\lambda_{bar} = \frac{\sum_{i=400}^{700} \lambda_i T_{canon}(\lambda_i) T_{filter}(\lambda_i)}{T_{total}}. \tag{6}$$

The application of Eqs. (5) and (6) to all the six available *Wratten* filters leads to the following barycentric wavelengths:

1. $\lambda_{bar,N.35}$= 437.8 nm;
2. $\lambda_{bar,N.47}$= 449.4 nm;
3. $\lambda_{bar,N.11}$= 536.6 nm;
4. $\lambda_{bar,N.12}$= 580.7 nm;
5. $\lambda_{bar,N.21}$= 602.1 nm;
6. $\lambda_{bar,N.33}$= 647.2 nm.

Therefore, the refractive indices computed using these filters are associated with the barycentric wavelengths listed above. Figure 4 shows an example of photos for each fluid and for every filter taken into account.

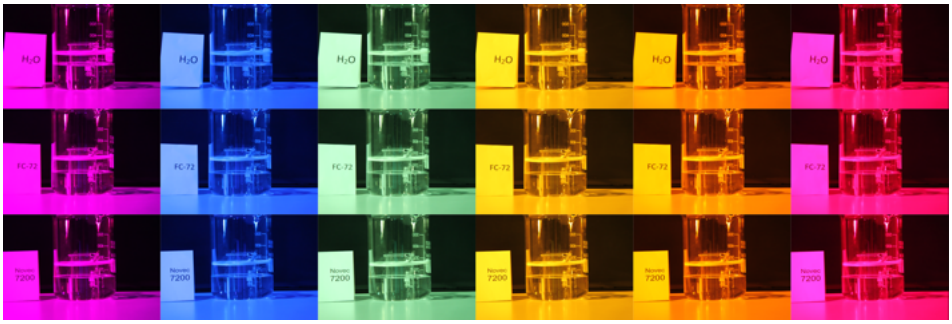

Fig. 4. Photos of the set-up arrangement for the liquids refractive index estimation. From top to bottom: pure water, FC-72, Novec7200; from left to right: $\lambda_{bar,N.35}$, $\lambda_{bar,N.47}$, $\lambda_{bar,N.11}$, $\lambda_{bar,N.12}$, $\lambda_{bar,N.21}$, $\lambda_{bar,N.33}$.

The spectral evaluation of the refractive index has been conducted by taking ten photos per filter and, for each photo, twenty measurements of $d_{C'}$. The registered temperature was around 25°C.

Optical Materials EXPRESS

2.3. Refractive index thermal variation

The variation of the fluorine liquids refractive index with temperature has been analyzed using the same method employed for the calculation of the spectral one, but, instead of considering the entire visible range, only the filter N.12 has been used: the temperature variation is then associated to the barycentric wavelength of 580.7 nm. In order to thermally characterize the refractive index, a domestic freezer has been used to cool the liquid sample below the room temperature (about 24-25°C). In this way, it was possible to reach a temperature of about -10°C. Therefore, the temperature range taken into account during the experiment is [-10, +25]°C. With the aid of the waterproof digital thermometer SDT 319 (resolution 0.1°C), the liquid temperature has been monitored regularly and recorded for every increase of 5°C. For each registered temperature, a set of ten photos has been taken and twenty measurements carried out per photo.

2.4. Transparency evaluation

The transparency calculation applied to a fluid implies the attainment of a quantity known as absorption coefficient α, a parameter, function of λ, indicating the wavelengths absorption of a mean per unit length of propagation. Multiplied for the liquid sample length, it gives the e-folding distance for attenuation of the intensity due to absorption, and, through the Lambert-Beer law, the transmissibility of the liquid sample of length L:

$$T_L = \exp(-\alpha L). \tag{7}$$

Note that Eq. (7) applies strictly only in the case of light normal incidence: such condition has been always satisfied during the measurements, hence justifying the employment of Eq. (7). From the evaluation of T_L, α can be measured by knowing the liquid sample length. In order to estimate the liquid transmissibility, the sample must be illuminated with a light beam of known intensity and wavelength and the light intensity exiting the sample must hence be measured. For this purpose, a proper vessel has to be filled with the liquid under test and sealed at the extremities using optical glass windows. Schematically, the experimental configuration that it's planned to be employed is depicted in Fig. 5.

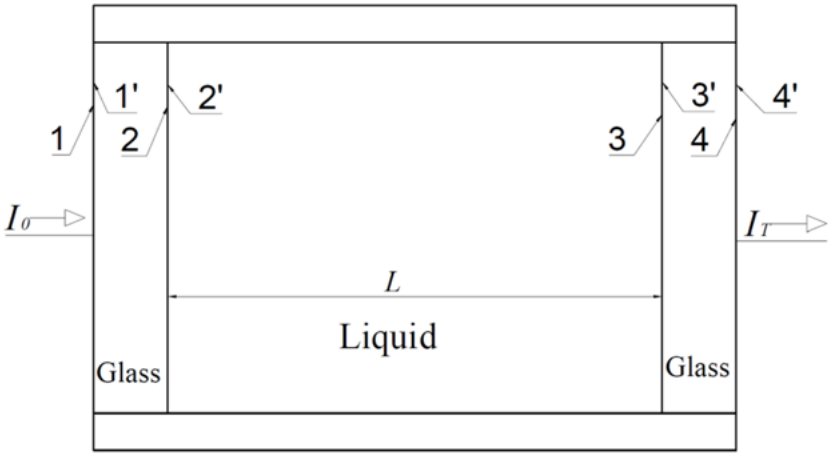

Fig. 5. Schematic representation of the liquid transparency evaluation set-up.

In Fig. 5, I_0 represents the intensity reaching the experimental assembly, I_T the intensity exiting the assembly itself, while the numbers 1, 2, 3 and 4 denote the interface surfaces separating means with different refractive indices. The intensity of the transmitted radiation I_T can be

Optical Materials EXPRESS

calculated with the relation:

$$I_T = \frac{I_T}{I_4}\frac{I_4}{I_{3'}}\frac{I_{3'}}{I_3}\frac{I_3}{I_{2'}}\frac{I_{2'}}{I_2}\frac{I_2}{I_{1'}}\frac{I_{1'}}{I_0}I_0, \tag{8}$$

where $\frac{I_{1'}}{I_0}$, $\frac{I_{2'}}{I_2}$, $\frac{I_{3'}}{I_3}$ and $\frac{I_T}{I_4}$ are the transmissibilities which can be computed from the Fresnel law for normal incidence between media with different refractive index, $\frac{I_2}{I_{1'}}$ and $\frac{I_4}{I_{3'}}$ are the transmissibilities which derive from the Lambert-Beer law quantifying the light absorption operated by the glass windows (noted that multiple reflections within the these windows are neglected), while $\frac{I_3}{I_{2'}}$ is the quantity indicated in Eq. (7) with T_L, namely the liquid transmissibility. Equation (8) can be re-written as:

$$I_T = BT_L I_0, \tag{9}$$

with $B = \frac{I_T}{I_4}\frac{I_4}{I_{3'}}\frac{I_{3'}}{I_3}\frac{I_{2'}}{I_2}\frac{I_2}{I_{1'}}\frac{I_{1'}}{I_0}$ a quantity depending only on the refractive index of the liquid and optical windows glass and on the thickness of the windows themselves. Now, if one imagine to have two identical vessels, with the same glass extremities, but having different lengths, L_1 and L_2, from Eqs. (7) and (9), applied to both assemblies, the following ratio can be obtained:

$$\frac{I_{T_1}}{I_{T_2}} = \frac{T_{L_1}}{T_{L_2}} = \exp[-\alpha(L_1 - L_2)]. \tag{10}$$

The same light beam is considered illuminating both assemblies. The liquid absorption coefficient descends from Eq. (10):

$$\alpha = \frac{\ln\left(\frac{I_{T_1}}{I_{T_2}}\right)}{L_2 - L_1}. \tag{11}$$

Therefore, α depends only upon the logarithmic ratio between the exiting intensities I_{T_1} and I_{T_2} and the length difference of the assemblies, but it is not influenced by refractive index and thickness of the optical windows. Actually, since the latter always exhibit (small) differences between each others in terms of optical parameters and size, Eq. (11) need to be adjusted with a correction term. Following the procedure illustrated in Ref. [9], Eq. (11) can be re-written as:

$$\alpha = \frac{\ln\left(\frac{I_{T_1}}{I_{T_2}}\frac{I_{T_{e2}}}{I_{T_{e1}}}\right)}{L_2 - L_1}, \tag{12}$$

where the correction factor $\frac{I_{T_{e2}}}{I_{T_{e1}}}$ is given by the ratio of the exiting light intensities measured for the assembly of length L_2 and L_1 respectively in absence of liquid (the pedix e denotes the "empty" vessel). The experimental set-up, arranged in order to compute α from Eq. (12), comprises two 1 /2 inch diameter galvanized steel pipes, having only one threaded end and length of $L_1 = 20$ cm and $L_2 = 100$ cm respectively, two 1 mm thick BK7 optical windows and one 1 /2 inch diameter galvanized steel T-joint per each pipe. The T-joints, internally threaded and coupled with the pipes, have been employed to efficiently pour the liquid. After having cleaned pipes, joints and windows with isopropyl alcohol, all the threaded ends have been wrapped with Teflon and the optical windows glued to the pipes with silicone. As light sources, four laser have been used:

1. A class 3R red laser (JDS Uniphase), operating wavelength 633 nm, nominal power <4 mW;
2. A class 3R green laser (Thorlabs), operating wavelength 532 nm, nominal power 4.9 mW;
3. A class 3B green laser (Edmund Optics), operating wavelength 543 nm, nominal power 1.5 mW;
4. A class 3R blue laser (Thorlabs), operating wavelength 405 nm, nominal power <5 mW.

Optical Materials EXPRESS

A photodiode coupled to the S370 optometer (Graseby Optronics) was instead used for the measurement of the exiting power. In this regard, it's possible to notice that light intensity I and power P are connected by the following relation:

$$P = I\Omega, \tag{13}$$

being Ω the solid angle subtended by the observer. Keeping fixed the distances laser-pipes assembly and pipes assembly-detector and since the detector never changes during the experiment, it's possible to consider constant the solid angle subtended by the photodiode for all the measurements. Inserting Eq. (13) in Eq. (12), the estimation of the liquid absorption coefficient is then related directly to the measured powers by:

$$\alpha = \frac{\ln\left(\frac{P_{T_1}}{P_{T_2}}\frac{P_{T_{e2}}}{P_{T_{e1}}}\right)}{L_2 - L_1}. \tag{14}$$

P_{T_1} and $P_{T_{e1}}$ are the exiting powers measured for the pipe of length L_1 with and without the liquid respectively, while P_{T_2} and $P_{T_{e2}}$ represent the same quantity but for the pipe of length L_2. The final set-up is depicted in Fig. 6.

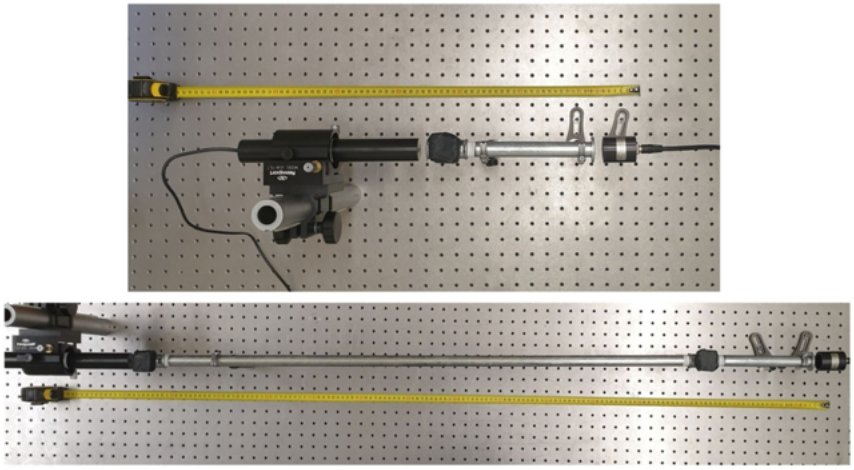

Fig. 6. Experimental set-up for the liquid absorption coefficient evaluation. Top: "short" liquid sample, $L_1 = 20$ cm; bottom: "long" liquid sample, $L_2 = 100$ cm.

Before the measurements were taken, the entire assembly was covered with a black sheet in order to avoid the interference with external light.

3. Results and discussion

The techniques described in Sec. 2 have been firstly tested using commercial pure water, for which refractive index and absorption coefficient estimations can be found in literature.

3.1. Pure water refractive index

The determination of the liquid refractive index is based upon Eq. (4), namely on the evaluation of the cylinder image diameter, $d_{C'}$, and the knowledge of the actual cylinder diameter, d_C. The latter has been measured 10 times with a digital caliper, obtaining $d_C = 42.01 \pm 0.01$ mm, being the uncertainty given by the associated standard deviation. For $d_{C'}$ instead, a total of 200 measurements have been carried out for each of the six barycentric wavelengths listed in Sec.

Optical Materials EXPRESS

2.2. The final estimation of n is then given by the ratio of the average diameters on the basis of Eq. (4), with an associated uncertainty provided by the errors propagation:

$$\Delta n = \sqrt{\left(\frac{\partial n}{\partial d_{C'}}\Delta d_{C'}\right)^2 + \left(\frac{\partial n}{\partial d_C}\Delta d_C\right)^2}, \tag{15}$$

with $\Delta d_{C'} = 3\sigma$, being σ the measurements standard deviation. In Table 1, the experimental values of pure water refractive index are listed.

Table 1. Pure water experimental refractive index at $T = 25$ °C.

Pure water	
λ_{bar} [nm]	n
437.8	1.3400 ± 0.0009
449.4	1.3392 ± 0.0008
536.6	1.3348 ± 0.0005
580.7	1.3332 ± 0.0005
602.1	1.3325 ± 0.0005
647.2	1.3313 ± 0.0006

The interpolation of the six values of n in the visible spectrum is performed with the two most common dispersion equations, namely the Sellmeier and the Cauchy ones. Their coefficients are determined with a non-linear least squares fitting. Based upon the summed squares of residuals (SSE), the adjusted R-square and the fit standard error (Root Mean Squared Error, RMSE), it was chosen to take into account a second-order Sellmeier equation and a second-order Cauchy one, hence:

$$n^2(\lambda) = 1 + \frac{A_1\lambda^2}{\lambda^2 - A_2} + \frac{A_3\lambda^2}{\lambda^2 - A_4}, \tag{16}$$

$$n^2(\lambda) = B_0 + \frac{B_1}{\lambda^2} + \frac{B_2}{\lambda^4}, \tag{17}$$

with $\lambda \in [400,700]$ nm. In Table 2, the Sellmeier and Cauchy coefficients are reported for pure water along with the merit functions taken into account.

In Fig. 7, the results obtained for pure water are presented as well. In this plot, also three reference curves, taken by Refs. [9] and [10] respectively, are shown for comparison: they present a very good agreement with the results of this work. In particular, the experimental data (denoted with blue circles) are comparable with the reference ones within the uncertainties, except for the Cauchy formula of Ref. [9], which predicts higher values of refractive index in the blue portion of the visible spectrum.

Therefore, the method employed in this work to determine the pure water dispersion gives results consistent with those reported in other studies and obtained using different approaches. This consistency is highlighted also by the Abbe number. Indeed, the latter:

$$V_d = \frac{n_d - 1}{n_F - n_C} \tag{18}$$

exhibits an average value of 55.86 for the formula derived in this work, 48.66 for the reference formula of Ref. [9] and 55.42 for the Ref. [10] one.

The thermal evaluation of the refractive index was carried out in a manner similar to the spectral one. For pure water, the temperature range considered is [+1,+25]°C in order to avoid solidification. Therefore, 200 measurements of $d_{C'}$ have been taken for each of the six recorded

Optical Materials EXPRESS

Table 2. Coefficients of Sellmeier and Cauchy fitting for pure water, with the error parameters RSME, SSE and R-adjusted.

Pure water			
Parameter	Sellmeier formula	Parameter	Cauchy formula
A_1	-63.61721	B_0	1.74993
A_2	-55.87186	$B_1(10^3)$	9.97976
A_3	64.37032	$B_2(10^8)$	-2.30831
A_4	72.01014	-	-
RMSE (10^{-5})	5.78763	RMSE (10^{-5})	0.99956
SSE (10^{-8})	2.00979	SSE (10^{-8})	0.05994
R-adjusted	0.99984	R-adjusted	0.99999

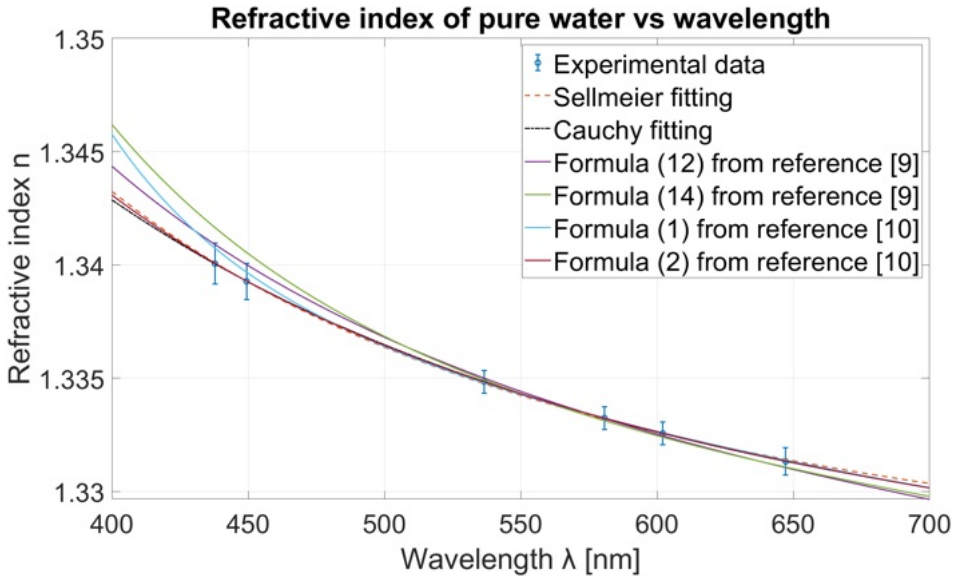

Fig. 7. Variation of pure water refractive index within the spectral range [400,700] nm. The blue circles represent the experimental data obtained in this work, while the dashed red and black curves the Sellmeier and Cauchy fitting respectively. For comparison, several dispersion curves, retrieved by Refs. [9] and [10], are reported with solid lines.

temperatures and n computed using Eq. (4). Table 3 shows the obtained results. In literature, it was possible to find a formula expressing the variation of the pure water refractive index with temperature. The latter, retrievable in Ref. [10] and employed as a reference for the thermal characterization, is actually a third-order polynomial equation in T (having fixed the working wavelength): a similar formula has been used to interpolate the experimental data. Hence:

$$n(T) = C_3T^3 + C_2T^2 + C_1T + C_0, \tag{19}$$

where the coefficients C_i are wavelength-dependant. The working wavelength is 580.7 nm.

The coefficient C_i are listed in Table 4, along with the parameters expressing the interpolation error budget.

A comparison between the experimental and the reference curves is instead reported in Fig. 8. As it can be deduced from the plot, also for the thermal characterization, the results of this work are in agreement (within the uncertainties) with the reference data.

Optical Materials EXPRESS

Table 3. Pure water experimental refractive index at $\lambda_{bar,N.12}$ = 580.7 nm.

Pure water	
T [°C]	n
1.0	1.3361 ± 0.0004
5.0	1.3360 ± 0.0003
10.0	1.3359 ± 0.0003
15.0	1.3355 ± 0.0004
20.0	1.3352 ± 0.0003
25.0	1.3348 ± 0.0004

Table 4. Coefficients of the third-order polynomial (Eq. (19)) for $\lambda_{bar,N.12}$ = 580.7 nm, with the error parameters RSME, SSE and R-adjusted.

Pure water	
Parameter	Third-order polynomial
C_0	1.33609
$C_1(10^{-6})$	5.68783
$C_2(10^{-6})$	-3.58731
$C_3(10^{-8})$	5.18518
RMSE (10^{-5})	3.43110
SSE (10^{-8})	0.70635
R-adjusted	0.99729

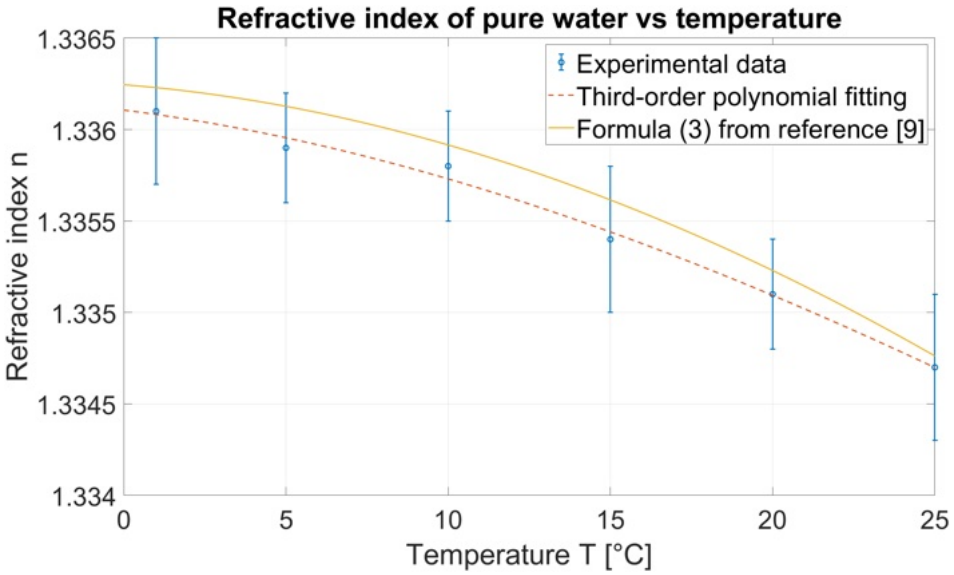

Fig. 8. Variation of pure water refractive index within the thermal range [+1,+25] °C. The blue circles represent the experimental data obtained in this work, while the dashed red curve the third-order polynomial fitting. For comparison, the reference data, retrieved by Ref. [10], are reported with the yellow solid line. Both curves refer to the working wavelength of 580.7 nm.

Optical Materials EXPRESS

These techniques were then applied to the fluorine fluids. The main results are described below.

3.2. FC-72 refractive index

In Table 5, the measured values of refractive index for FC-72 are shown.

Table 5. FC-72 experimental refractive index at T = 25 °C.

FC-72	
λ_{bar} [nm]	n
437.8	1.2529 ± 0.0007
449.4	1.2527 ± 0.0007
536.6	1.2516 ± 0.0004
580.7	1.2512 ± 0.0004
602.1	1.2509 ± 0.0004
647.2	1.2505 ± 0.0005

Such values have been then interpolated with the Sellmeier and Cauchy formulas (Eqs. (16) and (17) respectively): their spectral variation and main parameters are reported in Fig. 9 and Table 6 respectively.

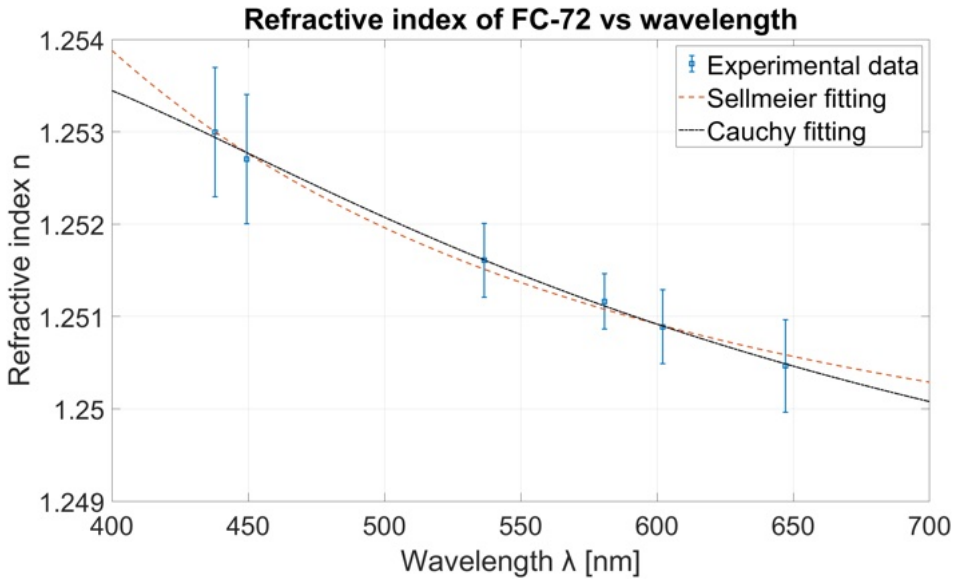

Fig. 9. Variation of FC-72 refractive index within the spectral range [400,700] nm. The blue squares represent the experimental data obtained in this work, while the dashed red and black curves the Sellmeier and Cauchy fitting respectively.

A quick comparison between Tables 2 and 6 reveals that the Sellmeier equation interpolates pure water and FC-72 experimental data with the same degree of approximation since RMSE and SSE present the same order of magnitude; the second-order Cauchy equation, instead, is much more accurate for pure water since RMSE and SSE are respectively one and two order of magnitude lesser than the corresponding FC-72 values (which, however, remain remarkably low).

Optical Materials EXPRESS

Table 6. Coefficients of Sellmeier and Cauchy fitting for FC-72, with the error parameters RSME, SSE and R-adjusted.

FC-72			
Parameter	Sellmeier formula	Parameter	Cauchy formula
A_1	-32.27361	B_0	1.55551
A_2	-25.41061	$B_1(10^3)$	4.01737
A_3	32.83247	$B_2(10^8)$	-2.42996
A_4	40.10746	-	-
RMSE (10^{-5})	7.71714	RMSE (10^{-5})	4.29073
SSE (10^{-8})	3.57325	SSE (10^{-8})	1.10462
R-adjusted	0.99652	R-adjusted	0.99892

The average Abbe number is 144.75. The FC-72 fluorine fluid is therefore characterized by a spectral dispersion around 2.5 lesser than the pure water one: passing from 437.8 to 647.2 nm, the pure water refractive index undergoes a relative reduction of 0.65%, while for FC-72 such decrease is around 0.2%.

Regarding the thermal characterization, instead, unlike for pure water, the temperature range considered is [-10,+25]°C, being the fluorine fluids solidification temperature much more lower than the water one (around -90°C). The interpolation of the experimental data listed in Table 7 was carried out using the third-order polynomial (Eq. (19)), whose coefficients are reported in Table 8 with the associated statistics.

Table 7. FC-72 experimental refractive index at $\lambda_{bar,N.12}$ = 580.7 nm.

FC-72	
T [°C]	n
-10.0	1.2661 ± 0.0004
-5.0	1.2637 ± 0.0005
0.0	1.2613 ± 0.0004
5.0	1.2588 ± 0.0003
10.0	1.2562 ± 0.0005
15.0	1.2535 ± 0.0005
20.0	1.2521 ± 0.0004
25.0	1.2510 ± 0.0004

A visual representation of the FC-72 refractive index thermal evolution is depicted in Fig. 10. A comparison between Figs. 8 and 10 clearly shows that the increase of n with the decreasing of T is much more pronounced for FC-72 with respect to pure water. Indeed, passing from 25 to around 0°C, the fluorine fluid refractive index increases of around 0.8%, while for pure water such increase is around 0.1%.

This could be due to the different coefficient of thermal expansion (CTE): the fluorine fluids have a CTE one order of magnitude higher than the pure water one, therefore they are subjected to a more significant change in volume and, therefore, in density, than water for a same temperature variation.

3.3. Novec7200 refractive index

In Table 9, the measured values of refractive index for Novec7200 are shown.

Optical Materials EXPRESS

Table 8. Coefficients of the third-order polynomial (Eq. (19)) for $\lambda_{bar,N.12}$ = 580.7 nm, with the error parameters RSME, SSE and R-adjusted.

FC-72	
Parameter	Third-order polynomial
C_0	1.2613
$C_1(10^{-4})$	-5.2877
$C_2(10^{-6})$	-2.8834
$C_3(10^{-7})$	3.0178
RMSE (10^{-4})	1.5699
SSE (10^{-7})	1.4788
R-adjusted	0.9997

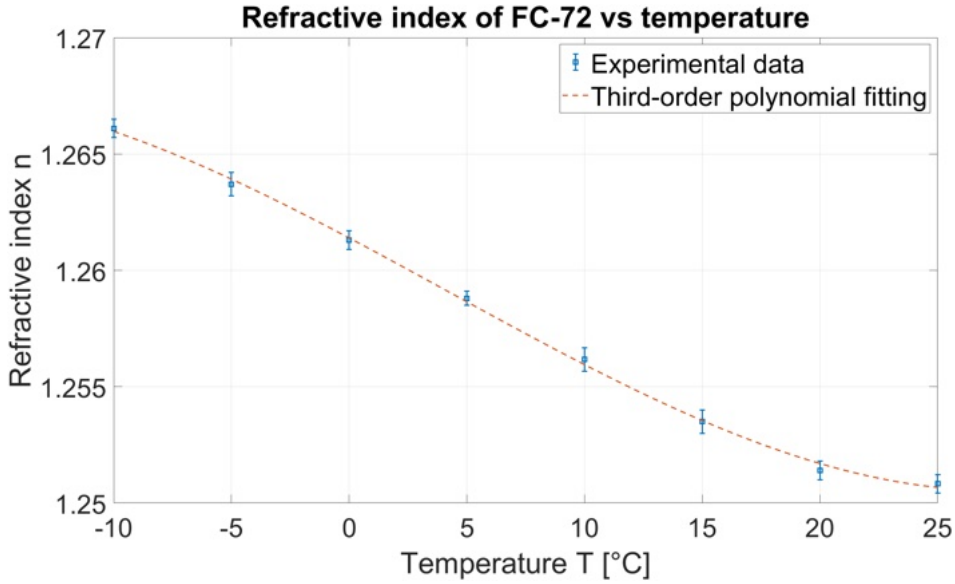

Fig. 10. Variation of FC-72 refractive index within the thermal range [-10,25] °C and for $\lambda_{bar,N.12}$ = 580.7 nm. The blue squares represent the experimental data obtained in this work, while the dashed red curve the third-order polynomial fitting.

Table 9. Novec7200 experimental refractive index at T = 25 °C.

Novec7200	
λ_{bar} [nm]	n
437.8	1.2837 ± 0.0007
449.4	1.2829 ± 0.0006
536.6	1.2813 ± 0.0004
580.7	1.2807 ± 0.0004
602.1	1.2801 ± 0.0004
647.2	1.2796 ± 0.0005

Optical Materials EXPRESS

Such values have been then interpolated with the Sellmeier formula (Eq. (16)) and the Cauchy one (Eq. (17)): their spectral change and main parameters are reported in Fig. 11 and Table 10 respectively.

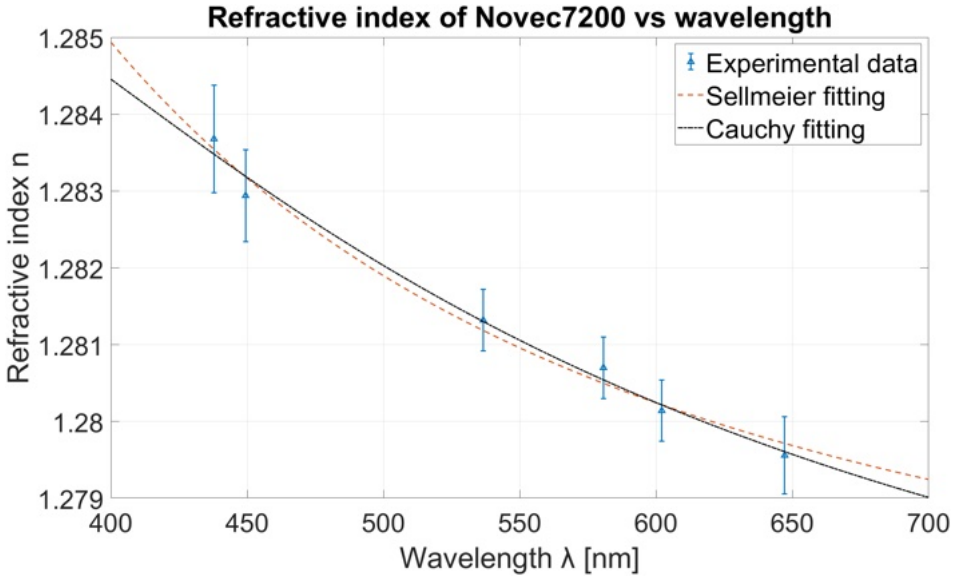

Fig. 11. Variation of Novec7200 refractive index within the spectral range [400,700] nm. The blue triangles represent the experimental data obtained in this work, while the dashed red and black curves the Sellmeier and Cauchy fitting respectively.

Table 10. Coefficients of Sellmeier and Cauchy fitting for Novec7200, with the error parameters RSME, SSE and R-adjusted.

Novec7200			
Parameter	Sellmeier formula	Parameter	Cauchy formula
A_1	-41.34046	B_0	1.62553
A_2	-33.91759	$B_1(10^3)$	5.63743
A_3	41.96985	$B_2(10^8)$	-2.80132
A_4	49.17317	-	-
RMSE (10^{-5})	16.68654	RMSE (10^{-5})	15.05197
SSE (10^{-8})	16.70645	SSE (10^{-8})	13.59371
R-adjusted	0.99357	R-adjusted	0.99477

The average Abbe number is 103.71. For Novec7200, the degree of error due to interpolation in terms of RMSE and SSE is one order of magnitude greater, both for Sellmeier and Cauchy equations, than FC-72 one (the accuracy of the interpolation remaining acceptable). The dispersion is limited, as demonstrated by the average value of V_d: the relative decrease of n passing from 437.8 to 647.2 nm is around 0.32%.

Also in this case, the thermal characterization was performed considering the temperature range [-10,+25]°C. The experimental data are listed in Table 11.

The main parameters of the interpolation, carried out with Eq. (19), are reported in Table 12.

Figure 12 shows, instead, the Novec7200 refractive index thermal variation.

Optical Materials EXPRESS

Table 11. Novec7200 experimental refractive index at $\lambda_{bar,N.12}$ = 580.7 nm.

Novec7200	
T [°C]	n
-10.0	1.2951 ± 0.0004
-5.0	1.2925 ± 0.0005
0.0	1.2907 ± 0.0005
5.0	1.2877 ± 0.0003
10.0	1.2854 ± 0.0004
15.0	1.2835 ± 0.0004
20.0	1.2819 ± 0.0004
25.0	1.2811 ± 0.0004

Table 12. Coefficients of the third-order polynomial (Eq. (19)) for $\lambda_{bar,N.12}$ = 580.7 nm, with the error parameters RSME, SSE and R-adjusted.

Novec7200	
Parameter	Third-order polynomial
C_0	1.2903
$C_1(10^{-4})$	-5.0195
$C_2(10^{-6})$	-8.4749
$C_3(10^{-7})$	2.4580
RMSE (10^{-4})	2.1924
SSE (10^{-7})	2.8839
R-adjusted	0.9992

As FC-72, also Novec7200 exhibits a refractive index thermal variation higher than the pure water one for a certain ΔT, likely as a consequence of its higher coefficient of thermal expansion.

3.4. Absorption coefficient estimation

The transparency evaluation is carried out with the methodology described in Sec. 2.4. As for refractive index, the absorption coefficient was firstly estimated for pure water, for which extensive references could be found in literature. In this work, Ref. [11] was used as reference. Operatively speaking, the following procedure was employed:

1. The laser and the detector have been fixed upon the optical bench. Their positions did not change during the experiment;
2. After a warm-up of 15 minutes, the laser actual power was measured in absence of any sample;
3. With the laser turned on, the empty cells of length L_1 was located between source and detector and properly aligned. The power $P_{T_{e1}}$ was then recorded every minute for 30 minutes;
4. The cell was hence filled with the fluid under test, paying attention to avoid air bubble in the tube. The power P_{T_1} was then recorded every minute for 30 minutes;
5. The points 3. and 4. were repeated for the cell of length L_2, obtaining $P_{T_{e2}}$ and P_{T_2};

Optical Materials EXPRESS

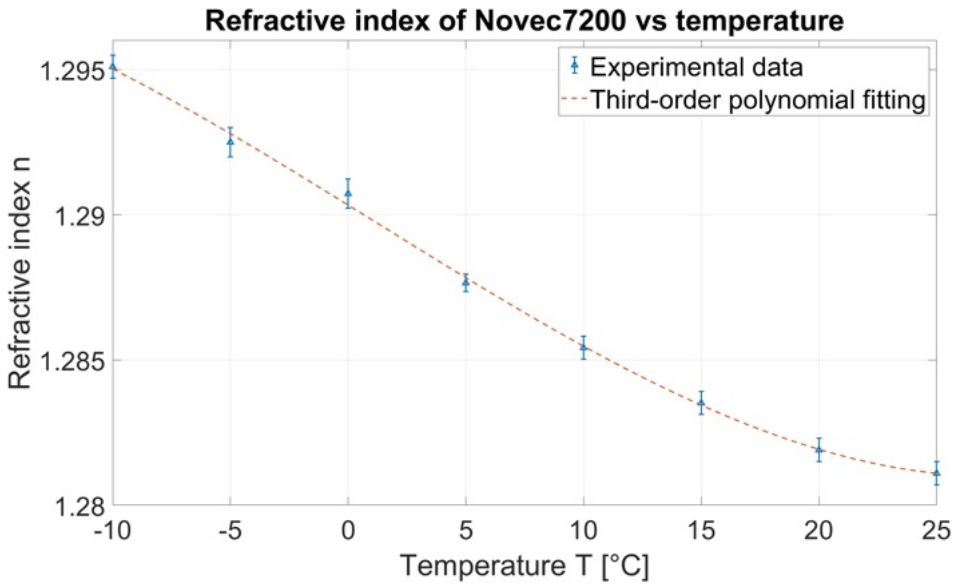

Fig. 12. Variation of Novec7200 refractive index within the thermal range [-10,+25] °C. The blue squares represent the experimental data obtained in this work, while the dashed red curve the third-order polynomial fitting.

6. For each fluid, the entire procedure was repeated with the four lasers, one by one.

The final powers have been computed as the average of the corresponding values taken over time. The absorption coefficient was then computed with Eq. (14). The uncertainty associated with each power is given by 3σ, with σ being the measurements standard deviation. Applying the formula for the errors propagation:

$$\Delta\alpha = \sqrt{\left(\frac{\partial\alpha}{\partial P_{T_{e1}}}\Delta P_{T_{e1}}\right)^2 + \left(\frac{\partial\alpha}{\partial P_{T_1}}\Delta P_{T_1}\right)^2 + \left(\frac{\partial\alpha}{\partial P_{T_{e2}}}\Delta P_{T_{e2}}\right)^2 + \left(\frac{\partial\alpha}{\partial P_{T_2}}\Delta P_{T_2}\right)^2}, \tag{20}$$

also the uncertainty associated to α were eventually estimated. Given four data points to interpolate, it was chosen to select a third-order polynomial fitting for the estimation of the absorption coefficient variation in the visible range in order to reduce the fitting error to zero. The absorption coefficient can therefore be expressed by:

$$\alpha(\lambda) = D_3\lambda^3 + D_2\lambda^2 + D_1\lambda + D_0, \tag{21}$$

with $\lambda \in [400,700]$ nm. In Table 13 the experimental absorption coefficients for the three fluids taken into account are listed, along with the associated uncertainties, for the four laser sources working wavelengths.

In Table 14, instead, the coefficients D_i for the pure water, FC-72 and Novec7200 fitting polynomial are listed; in Fig. 13 a comparison between the experimental values listed in Table 13, interpolated with Eq. (21) using the coefficients enumerated in Table 14 for each liquid, is shown along with the reference data retrieved in Refs. [9] and [11] for pure water in the visible range.

From the plot of Fig. 13, it's possible to notice that the pure water absorption coefficient experimental values obtained in this work are comparable with the reference data and the corresponding fitting (represented with the dashed red curve) correctly describes the increasing evolution with λ in the visible spectrum, even if the peculiar absorption features are ignored.

Optical Materials EXPRESS

Table 13. Experimental values of absorption coefficient for pure water, FC-72 and Novec7200.

λ [nm]	Pure water α [cm^{-1}]	FC-72 α [cm^{-1}]	Novec7200 α [cm^{-1}]
405	$(8.833 \pm 3.883)\cdot10^{-5}$	$(9.703 \pm 5.362)\cdot10^{-5}$	$(1.489 \pm 0.389)\cdot10^{-4}$
532	$(5.782 \pm 1.990)\cdot10^{-4}$	$(1.536 \pm 0.988)\cdot10^{-4}$	$(2.581 \pm 1.022)\cdot10^{-4}$
543	$(7.094 \pm 2.709)\cdot10^{-4}$	$(1.616 \pm 0.864)\cdot10^{-4}$	$(2.752 \pm 0.829)\cdot10^{-4}$
633	$(2.960 \pm 0.313)\cdot10^{-3}$	$(3.562 \pm 1.218)\cdot10^{-4}$	$(7.304 \pm 1.315)\cdot10^{-4}$

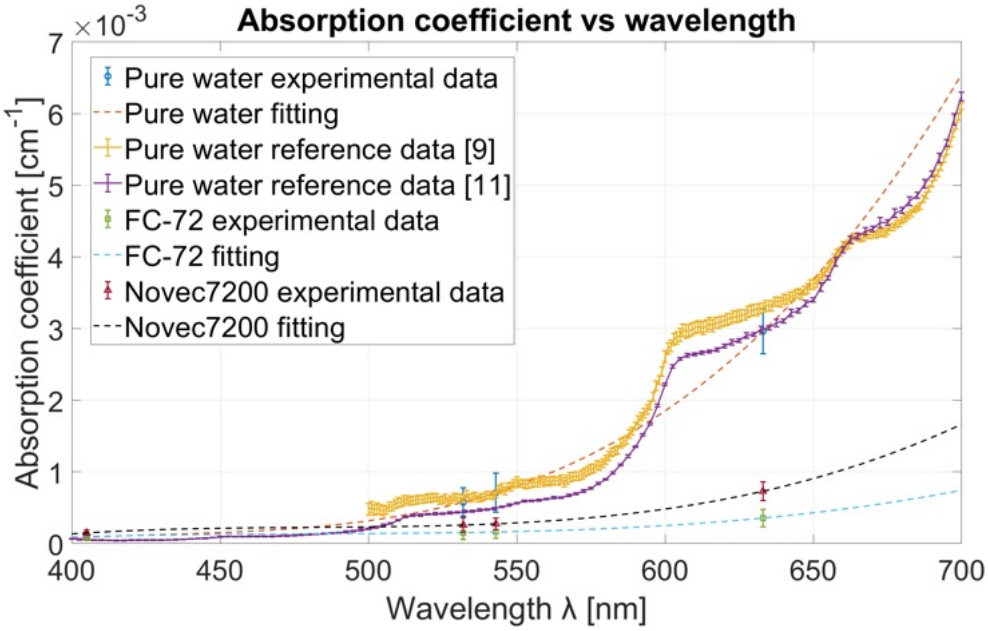

Fig. 13. Absorption coefficient experimental values of pure water (blue circles) and fluorine fluids FC-72 (green squares) and Novec7200 (red triangles) for four working wavelengths: 405, 532, 543 and 633 nm. In the plot, along with the third-order polynomial fitting for each liquid, also the pure water reference data retrieved from Refs. [9] and [11] are shown (with solid yellow and purple lines respectively) for comparison.

Table 14. Coefficients of the third order polynomial fitting (Eq. (21)) for pure water, FC-72 and Novec7200.

Parameter	Pure water	FC-72	Novec7200
$D_0(10^{-2})$	-2. 5341	-0.5877	-1.4369
$D_1(10^{-4})$	1.7480	0.3712	0.9056
$D_2(10^{-7})$	- 4.0280	-0.7683	-1.8789
$D_3(10^{-10})$	3.1166	0.5323	1.3033

The third order polynomial fitting, therefore, exhibits a double advantage: it allows reducing the fitting error to zero, while coherently representing, at the same time, the overall variation of the absorption coefficient, giving an estimate of the average values of α in the visible range.

However, there can be a slight mismatch between interpolated values and real ones, as highlighted in the case of the water sample: while our results are coherent with the literature results, the fitting at intermediate wavelengths slightly deviates from real values.

Optical Materials EXPRESS

If it can be hypothesized that the same considerations hold also for the fluorine fluids, namely that the fitting for FC-72 and Novec7200 (denoted with the cyan and black dashed curves respectively) provides their average value for each $\lambda \in [400,700]$, then it's immediate to observe their low degree of absorption, especially when compared to the pure water one for $\lambda > 500$ nm.

4. Conclusions

In this paper, the refractive index and absorption coefficient experimental quantification of two fluorine fluids, the commercially known FC-72 and Novec7200, has been carried out for the MezzoCielo application. In order to verify the reliability of the employed methodology, the pure water optical properties were firstly estimated and the results compared with the reference data retrieved in literature ([9,10] for refractive index and [9,11] for absorption coefficient). The fluorine liquids refractive index, experimentally obtained in the spectral range [400,700] nm, clearly shows an evolution which can be described (with sufficient accuracy) with the two most common dispersion formula, namely the Sellmeier and the Cauchy ones, and, apparently, it does not exhibit any "exotic" behaviour. Moreover, the dispersion of these fluids is limited, as demonstrated by their Abbe number, around 2.5 and 2 times higher than the pure water one for FC-72 and Novec7200 respectively. The liquids refractive index was also estimated in the temperature range [-10,+25]°C and it has been proved that its thermal variation can be accurately described by a third-order polynomial fitting. Moreover, it has been shown that the fluorine fluids exhibit an index change around 7-8 times greater than the pure water one passing from 0 to 25°C, probably as a consequence of their higher value of CTE.

The absorption coefficient of the fluids taken into account was measured for four working wavelengths and its variation inferred in the entire visible range. Unlike pure water, the fluorine liquids show a visible light absorption which increases moderately passing from 400 to 700 nm: in particular, for $\lambda = 633$ nm the pure water absorption coefficient is one order of magnitude greater than the fluorine fluids one. On the basis of Eq. (7), for a same optical path, the latter higher performance in terms of transparency can therefore be deduced. The employment of one of them as optical fluid for the MezzoCielo telescope can hence be considered confirmed, especially FC-72, whose transparency, the highest among the three liquids examined in this work, may allow the realization of telescopes characterized by high equivalent diameters.

Disclosures. The authors declare no conflicts of interest.

Data availability. Data underlying the results presented in this paper are not publicly available at this time but may be obtained from the authors upon reasonable request.

References

1. R. Ragazzoni, M. Dima, C. Arcidiacono, *et al.*, "Mezzocielo: an attempt to redesign the concept of wide field telescopes," in *Ground-based and Airborne Telescopes VIII*, vol. 11445 H. K. Marshall, J. Spyromilio, and T. Usuda, eds., International Society for Optics and Photonics (SPIE, 2020), p. 1144534.
2. S. D. Rosa, R. Ragazzoni, D. Magrin, *et al.*, "Finite element analysis of the mezzocielo monocentric optical system and other mechanical issues," in *Ground-based and Airborne Telescopes IX*, vol. 121823S (2022), p. 78.
3. S. D. Rosa, R. Ragazzoni, M. Dima, *et al.*, "Thermo-mechanical sizing and stress-induced birefringence analysis for the mezzocielo assembly," Journal of Astronomical Telescopes, Instruments, and Systems (JATIS) (2024). [Under revision].
4. 3M, "3m™ fluorinert™ electronic liquid fc-72," https://multimedia.3m.com/mws/media/64892O/3m-fluorinert-electronic-liquid-fc72-en.pdf.
5. 3M, "3m™ novec™ 7200 engineered fluid," https://multimedia.3m.com/mws/media/199819O/3m-novec-7200-engineered-fluid-en.pdf?&fn=prodinfo_nvc7200.pdf.
6. Y.-K. An, "Simple method to measure the refractive index of liquid with graduated cylinder and beaker," Rev. Sci. Instrum. **88**(12), 12515 (2017).
7. https://kolarivision.com/articles/internal-cut-filter-transmission.
8. J. Allie C. Peed, "Transmission of wratten filters," The Eastman Kodak Company.
9. S. Kedenburg, M. Vieweg, T. Gissibl, *et al.*, "Linear refractive index and absorption measurements of nonlinear optical liquids in the visible and near-infrared spectral region," Opt. Mater. Express **2**(11), 1588–1611 (2012).

Optical Materials EXPRESS

10. A. N. Bashkatov and E. A. Genina, "Water refractive index in dependence on temperature and wavelength: A simple approximation," Proc. SPIE **5068**, 393–395 (2003).
11. R. M. Pope and E. S. Fry, "Absorption spectrum (380–700 nm) of pure water. ii. integrating cavity measurements," Appl. Opt. **36**(33), 8710–8723 (1997).